Applied Physics Letters

Parameter-free determination of the exchange constant in thin films using magnonic patterning

Cite as: Appl. Phys. Lett. **108**, 102402 (2016); https://doi.org/10.1063/1.4943228
Submitted: 23 September 2015 . Accepted: 14 February 2016 . Published Online: 07 March 2016

M. Langer, K. Wagner, T. Sebastian, R. Hübner, J. Grenzer, Yutian Wang, T. Kubota, T. Schneider, S. Stienen, K. Lenz, H. Schultheiß, J. Lindner, K. Takanashi, R. E. Arias, and J. Fassbender

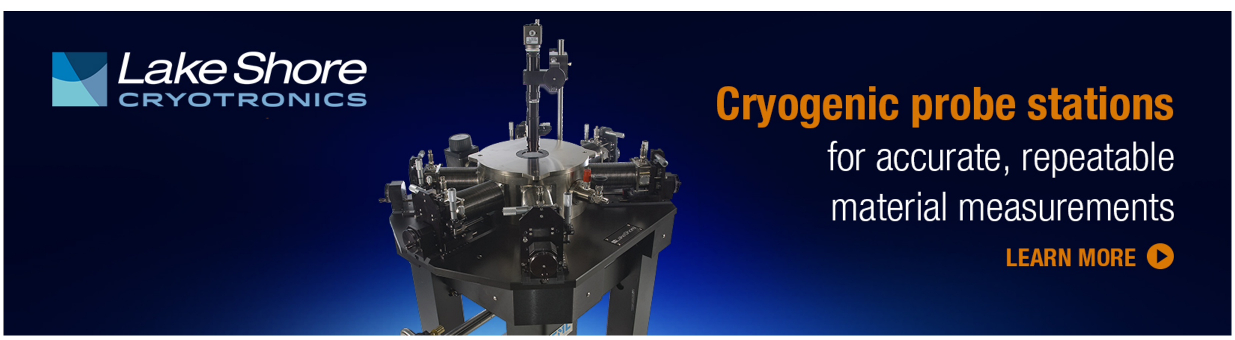

Parameter-free determination of the exchange constant in thin films using magnonic patterning

M. Langer,[1,2] K. Wagner,[1,2] T. Sebastian,[1] R. Hübner,[1] J. Grenzer,[1] Yutian Wang,[1] T. Kubota,[3] T. Schneider,[1,4] S. Stienen,[1] K. Lenz,[1] H. Schultheiß,[1] J. Lindner,[1] K. Takanashi,[3] R. E. Arias,[5] and J. Fassbender[1,2]

[1]*Helmholtz-Zentrum Dresden–Rossendorf, Institute of Ion Beam Physics and Materials Research, Bautzner Landstr. 400, 01328 Dresden, Germany*
[2]*Institute for Physics of Solids, Technische Universität Dresden, Zellescher Weg 16, 01069 Dresden, Germany*
[3]*Institute for Materials Research, Tohoku University, Sendai 980-8577, Japan*
[4]*Department of Physics, Technische Universität Chemnitz, Reichenhainer Str. 70, 09126 Chemnitz, Germany*
[5]*Departamento de Física, CEDENNA, FCFM, Universidad de Chile, Casilla 487-3, Santiago, Chile*

(Received 23 September 2015; accepted 14 February 2016; published online 7 March 2016)

An all-electrical method is presented to determine the exchange constant of magnetic thin films using ferromagnetic resonance. For films of 20 nm thickness and below, the determination of the exchange constant A, a fundamental magnetic quantity, is anything but straightforward. Among others, the most common methods are based on the characterization of perpendicular standing spin-waves. These approaches are however challenging, due to (i) very high energies and (ii) rather small intensities in this thickness regime. In the presented approach, surface patterning is applied to a permalloy ($Ni_{80}Fe_{20}$) film and a $Co_2Fe_{0.4}Mn_{0.6}Si$ Heusler compound. Acting as a magnonic crystal, such structures enable the coupling of backward volume spin-waves to the uniform mode. Subsequent ferromagnetic resonance measurements give access to the spin-wave spectra free of unquantifiable parameters and, thus, to the exchange constant A with high accuracy. © *2016 AIP Publishing LLC*. [http://dx.doi.org/10.1063/1.4943228]

For investigations as well as applications in the fields of spintronics and magnonics, the exact knowledge of either the exchange constant A or the corresponding exchange stiffness $D = 2A/M_S$ (with M_S the saturation magnetization) is essential. The reason is that most of today's applications are based on the *dynamics* of the magnetization built up by the microscopic spin system. Regarding the technical need to reduce the size of functional entities, exchange forces become dominant. Thus, the necessity for precise methods to determine the exchange constant becomes immediately evident.

There are several approaches[1,2] to determine the exchange constant of thin films with the most prevalent ones being (i) the magnetometric determination of the temperature-dependent decrease[3,4] of M_S and (ii) the investigation of spin-wave modes across the film thickness, referred to as perpendicular standing spin-waves (PSSWs) by either ferromagnetic resonance (FMR)[5,6] or Brillouin light scattering (BLS).[7–9] Approach (i) relies on thermal spin-wave excitation described by the Bloch-law, which becomes more complex and error-prone, if magnon-magnon processes are of relevance. In contrast, approach (ii) is based on the investigation of PSSW modes, which are shifted up to high energies and lowered in their intensities if the film thickness is very small.

A possible solution is presented based on frequency-dependent FMR measurements. After the characterization of the as-deposited film, a magnonic crystal is created by a periodical modulation of the surface. As shown for a variety of non-perturbative systems,[10–12] such structures enable a coupling of in-plane spin-wave modes to the uniform mode. Here, stripe-like perturbations are created on the film surface to couple spin-waves in backward volume (BV) geometry via two-magnon scattering (TMS)[13–15] to the uniform mode. In turn, such BV-modes allow for a straightforward calculation of A. This method is suited for many thin film systems and, additionally, yields most of the relevant magnetic properties. Advantages are the low energy of the BV modes as well as their high intensity due to the coupling to the uniform mode facilitated by FMR.

Altering the demagnetizing field, the perturbations act as scattering centers for the uniform mode with

$$\left(\frac{\omega}{\gamma}\right)^2 = \mu_0 H_0 \times (\mu_0 H_0 + \mu_0 M_{\mathrm{eff}}), \tag{1}$$

where $f = \omega/(2\pi)$ is the FMR frequency, $\mu_0 M_{\mathrm{eff}} = \mu_0 M_S - 2K_{2\perp}/M_S$ is the effective magnetization with $K_{2\perp}$ the uniaxial perpendicular anisotropy constant, and $\gamma = g\mu_B/\hbar$ is the gyromagnetic ratio (g is the g-factor). Being an elastic scattering process, TMS couples the uniform $\vec{k} = 0$ mode to higher $\vec{k} \neq 0$ modes. This requires for an energy- and momentum conservation. In fact, spin-wave modes degenerate with the uniform mode can be found for BV geometry with $\vec{k}_\parallel \| \vec{M}$ and $\vec{k}_\parallel$ the in-plane wave vector due to their parabolic dispersion[16] given by

$$\left(\frac{\omega}{\gamma}\right)^2 = \left(\mu_0 H_0 + Dk^2\right) \times \left[\mu_0 H_0 + Dk^2 + \mu_0 M_{\mathrm{eff}} F_{pp}\left(k_\parallel d\right)\right] \tag{2}$$

with d the film thickness, $\vec{k} = \vec{k}_\parallel + \vec{k}_\perp = \vec{k}_\parallel + p\pi/d \times \hat{e}_\perp$ ($p = 1, 2, 3, \ldots$) the spin-wave propagation vector and $F_{pp}(k_\parallel d) = [1 - \exp(-k_\parallel d)]/(k_\parallel d)$ the matrix element of the dipolar interaction. Momentum transfer is provided by the perturbations acting as scattering centers and TMS occurs if

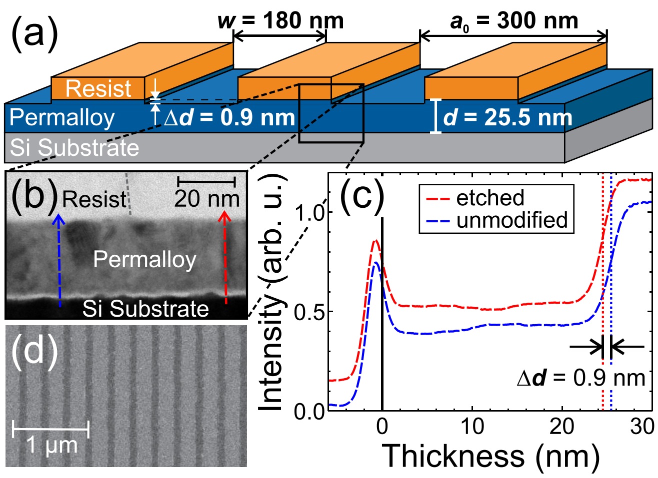

FIG. 1. (a) Sketch of a surface-modulated permalloy film. (b) Cross-sectional TEM image. The height modulation of the film is hardly visible on this scale. (c) A detailed TEM-study, as described in Ref. 17, proves a height modulation of $\Delta d = 0.9$ nm. (d) Top-view of the resist mask by scanning electron microscopy.

the scattering condition $k_\parallel = n \times 2\pi/a_0$ ($n = 1, 2, 3,\ldots$) is satisfied with a_0 the modulation periodicity. In this case, the uniform mode probed by FMR couples to the crossing BV modes and splits up in two branches referred to as optical (acoustical) mode for the high (low) frequency branch. For the crossing points (CPs), $\omega(k=0) = \omega(k \neq 0)$ applies, leading to the expression

$$D(H_n) = \left(\frac{a_0}{2\pi n}\right)^2 \times \left\{ \left[(\mu_0 H_n)^2 + \frac{1}{4}\mu_0^2 M_{\mathrm{eff}}^2 F_{pp}^2(k_\parallel d) + \mu_0^2 M_{\mathrm{eff}} H_n \right]^{\frac{1}{2}} - \mu_0 H_n - \frac{1}{2}\mu_0 M_{\mathrm{eff}} F_{pp}(k_\parallel d) \right\} \quad (3)$$

for the exchange stiffness D depending on the field value H_n of the nth CP (a derivation is provided in Ref. 17). Note that Eq. (3) represents the simple case of materials with negligible intrinsic anisotropy. In case of pronounced grooves, a uniaxial shape anisotropy $K_{2\parallel}$ needs to be taken into account and $\mu_0 H_n$ must be replaced by the term $\mu_0 H_n + 2K_{2\parallel}/M_S$.

In the following, the method is tested on two materials: (i) a 25.5 nm thick permalloy ($Ni_{80}Fe_{20}$) film and (ii) an 18.4 nm thick Heusler-compound $Co_2Fe_{0.4}Mn_{0.6}Si$ (CFMS). The former was chosen as a well-known system to prove the accuracy of the method. The latter was selected to show the applicability to technically relevant materials.[18–21]

The permalloy film was deposited on surface-oxidized Si(100) substrate by electron beam physical vapor deposition (EBPVD) carried out at a pressure of 2.6×10^{-6} mbar. Details of the epitaxial growth and magnetic properties of CFMS can be found in Refs. 22–24. The stack consists of a 20 nm Cr layer and a 40 nm Ag film acting as a buffer between the MgO(100) substrate and the $L2_1$ ordered CFMS. Besides, a 3 nm Ta cap layer was put on top of the stack. The surfaces of both films were stripe-patterned using e-beam lithography (EBL) and ma-N 2401 negative resist. The stripes have a nominal width of $b^{\mathrm{Py}} = 120$ nm and $b^{\mathrm{CFMS}} = 140$ nm, respectively, and a periodicity of $a_0 = 300$ nm [see Figs. 1(a) and 1(d)]. The structures were etched using 200 eV reactive (Ar) ion beam etching (RIBE) introducing surface perturbations as shown in Figs. 1(b) and 1(c). The etching depth of both magnetic films was below 1 nm. For a sub-nanometer etching underneath the Ta-cap (in case of CFMS), multiple 10 s etching steps were carried out with subsequent FMR measurements until mode-splitting was observed. A detailed thickness- and perturbation height analysis (values given in Table I) is provided in Ref. 17. The magnetic characterization was carried out using a 0.1–50 GHz vector network analyzer - ferromagnetic resonance (VNA-FMR) setup as described in Ref. 25. The sample was mounted flip-chip on a coplanar waveguide (width 80 μm), and the complex transmission parameter S_{21} was measured by the VNA as the FMR signal. The $f(H_0)$-dependencies were obtained by fitting multiple field-swept measurements.

In order to determine all magnetic parameters in Eq. (3), except from n and H_n, an FMR pre-characterization was carried out. Fitting the data of in-plane and out-of-plane $f(H_0)$ measurements,[17] g-factors and M_{eff} of both materials were determined and are shown in Table I. To exclude the presence of out-of-plane anisotropies, vibrating sample magnetometry (VSM) was employed to determine M_S (see Table I). Moreover, the films were checked for in-plane anisotropies revealing a weak uniaxial anisotropy $K_{2\parallel}/M_S = 0.12$ mT of the permalloy sample (subsequently neglected) and a fourfold anisotropy of $K_{4\parallel}/M_S = 0.95$ mT in case of CFMS.

As shown in Fig. 2(a), the $f(H_0)$ of the patterned permalloy film was measured with an in-plane field orientation along the modulation direction. Four resonance branches are visible separated by three CPs of the $n = 1$, 2, and 3 BV modes with the uniform mode, respectively. In principle, two effects can be observed: (i) A clear mode-splitting with an optical and acoustical branch close to the CP if the mode-separation is large compared to the linewidth. In the measurement, this is the case for the 1st and 3rd CPs. (ii) An effective line-broadening is observed[14,25,26] if mode-splitting is small compared to the linewidth. This was found for the 2nd and 4th CPs [see Figs. 2(b) and 2(c)]. The results regarding the CP locations in the $f(H_0)$ measurement as well as the corresponding values of the exchange stiffness constant are provided in Table II.

In case (i), the field H_n of the nth CP is assumed to be located at the field value with minimal mode separation. Whereas in case (ii), the frequency f_n of the nth CP can be estimated by fitting the peak of the linewidth ΔH using a fit function based on a superposition of Gilbert damping and a Gaussian peak $\Delta H(f) = \Delta H_{\mathrm{inh}} + 4\pi\alpha f/(\sqrt{3}\gamma) + C/\sqrt{2\pi\sigma^2} \times \exp[-(f-f_n)^2/(2\sigma^2)]$ with C the Gaussian amplitude and σ the standard deviation. Here, the center of the Gaussian indicates the frequency f_n and with Kittel's law [Eq. (1)], the respective field value H_n is found. Note that for a reduction of the fitting parameters, the Gilbert parameter $\alpha = 7.4 \times 10^{-3}$ and the inhomogeneous line broadening $\mu_0 \Delta H_{\mathrm{inh}} = 0.13$ mT of the uniform mode were used with field perpendicular to the modulation [gray asterisks in Figs. 2(b) and 2(c)].

TABLE I. Properties of the permalloy and the CFMS film.

Material	$g_\perp$	$g_\parallel$	$\mu_0 M_{\mathrm{eff}}$ (mT)	$\mu_0 M_S$ (mT)	A (pJ/m)	d (nm)	Δd (nm)
Py	2.106	2.112	924	925	8.7(4)	25.5(5)	0.9
CFMS	2.036	2.054	1387	1368	17.5(1.4)	18.4(5)	<0.5

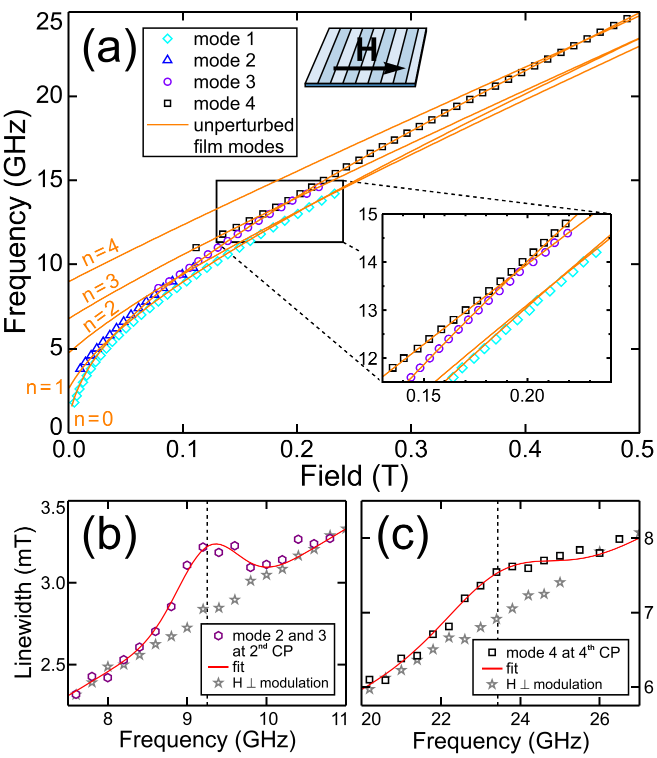

FIG. 2. (a) Frequency dependence of a surface-modulated permalloy sample with properties according to Table I. Orange lines indicate modes calculated using Eqs. (2) and (1), where $n=0$ indicates the uniform mode. (b) and (c) Plots of the linewidth at the second and fourth CP, respectively. The dashed lines indicate the center frequency of the Gaussian fit. Note that both peaks of the linewidth occur due to the presence of two very closely lying resonance peaks.

Clearly, the strong mode splitting at the 1st CP makes the determination of A more error-prone. Here, mode splitting is so pronounced, that mode 2 [blue triangles in Fig. 2(a)] is shifted causing a significant deviation of the value of D when the 2nd CP is used (23.8 T nm^2). However, the 3rd and 4th CPs allow for a precise determination of the exchange [stiffness] constant and coherently reveal $A = 8.7(4)$ pJ m^{-1} [$D = 23.6(1.2)$ T nm^2]. This value is consistent with available literature.[1,27,28] Note that the result was obtained taking into account an additional out-of-plane anisotropy of $K_{2\perp}/M_S = 5.3$ mT (see Ref. 17), which is very small compared to M_S. Since the method is sensitive to the film thickness d as well as the exchange stiffness D, both parameters can also be fitted. Here, the best fit was achieved for $D = 24.4$ T nm^2 and $d = 26.6$ nm, which is in very good agreement with the value found in the thickness analysis in Ref. 17.

A similar procedure was carried out for the CFMS film. The properties according to the pre-characterization are given in Table I. The $f(H_0)$ measurement of the patterned film [depicted in Fig. 3(a)] shows two modes [quasi-BV mode (quasi-uniform mode)—blue circles (black squares)] in the frequency ranges of 6.0–8.6 GHz and 11.3–13.3 GHz. Here, the splitting between optical and acoustical branch is very small, and thus, both modes could not be distinguished close to the CP. In Fig. 3(a), the part of the optical (acoustical) mode with energy below (above) the CP is referred to as quasi-BV mode. In-turn, the quasi-uniform mode denotes the optical (acoustical) mode with energy above (below) the CP.

TABLE II. Crossing points $f_n(H_n)$ and the corresponding spin-wave number n gained from an $f(H_0)$ measurement of surface modulated permalloy [see Fig. 2(a)]. Column 5 indicates whether the exchange stiffness in column 4 was determined using (i) the $f(H_0)$ mode-distance or (ii) the linewidth.

n	f_n (GHz)	$\mu_0 H_n$ (mT)	D (T nm^2)	Approach
1	(6.07)	(44.4)	(25.3)	(i)
2	9.26	96.1	23.8	(i) and (ii)
3	13.78	194.0	23.6	(i)
4	23.48	457.1	23.6	(ii)

To determine A, Eq. (2) was used to fit the 1st quasi-BV-mode using the material parameters gained in the pre-characterization (see Table I). The result is given by the red line in Fig. 3(a) revealing an exchange [stiffness] constant of $A = 17.5(1.4)$ pJ m^{-1} [$D = 32.2(2.6)$ T nm^2] and is consistent with the value [18(1) pJ m^{-1}] obtained by Sebastian *et al.* for 200 nm thick CFMS.[29]

In addition, numerical calculations (details provided in Ref. 17) of the FMR-response of a 5 nm CFMS film with 0.5 nm surface-modulation [shown in Fig. 3(b)] were carried out in order to test the applicability of the method to even thinner films. The mode-splitting at the 1st CP is depicted by the sequence of field-sweeps shown in Fig. 3(b). The corresponding amplitudes obtained by fitting are given in Fig. 3(c). In this thickness regime, an analysis of the mode amplitudes was found to be more appropriate compared to a linewdith- or resonance field analysis. Showing an intersection at the CP, the amplitudes reveal a CP-frequency of 28.23 GHz, and thus, an exchange stiffness of 32.9 T nm^2 with only 2% deviation from the actual value (32.2 T nm^2) used as input.[17]

It is concluded that the presented approach allows for an exact determination of the exchange constant A in thin films using magnonic patterning. Consistently with the literature, FMR measurements yield values of the exchange [stiffness] constant of 8.7(4) pJ m^{-1} [23.6(1.2) T nm^2] for permalloy and 17.5(1.4) pJ m^{-1} [32.2(2.6) T nm^2] for CFMS. Moreover, numerical calculations indicate the principle applicability of the method to 5 nm films. Thus, the method is capable of studying film properties in a thickness regime, where

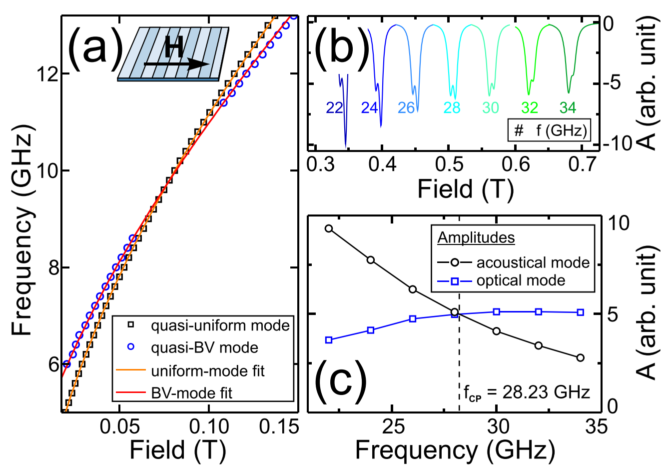

FIG. 3. (a) $f(H_0)$ dependence of an 18 nm surface modulated CFMS film with fits. (b) Numerically obtained field-sweeps of a 5 nm thick CMFS film with 0.5 nm surface modulation close to the 1st CP. (c) Resulting amplitudes for optical and acoustical mode obtained by fitting of each field-sweep shown in (b).

interfacial effects become relevant. As an all-electrical approach, this method is a sophisticated tool for the material characterization of a huge variety of structures, e.g., based on spin Hall effect (SHE)[30] or spin-transfer torque (STT).[31,32] It has been demonstrated that coupling phenomena, such as two-magnon scattering, can be employed to study spin-waves (such as backward volume modes), which in regular thin films cannot be detected by FMR.

We thank B. Scheumann for the film deposition. Support by the Nanofabrication Facilities Rossendorf at IBC is gratefully acknowledged. R.E.A. thanks CEDENNA FB0807, FONDECYT 1130192 (Chile). This work was funded by the DFG Grant LE2443/5-1.

[1]N. Smith, W. Doyle, D. Markham, and D. LaTourette, IEEE Trans. Magn. **23**, 3248 (1987).
[2]C. Eyrich, A. Zamani, W. Huttema, M. Arora, D. Harrison, F. Rashidi, D. Broun, B. Heinrich, O. Mryasov, M. Ahlberg, O. Karis, P. E. Jönsson, M. From, X. Zhu, and E. Girt, Phys. Rev. B **90**, 235408 (2014).
[3]L. Ritchie, G. Xiao, Y. Ji, T. Y. Chen, C. L. Chien, M. Zhang, J. Chen, Z. Liu, G. Wu, and X. X. Zhang, Phys. Rev. B **68**, 104430 (2003).
[4]R. Umetsu, A. Okubo, A. Fujita, T. Kanomata, K. Ishida, and R. Kainuma, IEEE Trans. Magn. **47**, 2451 (2011).
[5]P. E. Tannenwald and M. H. Seavey, Phys. Rev. **105**, 377 (1957).
[6]M. H. Seavey and P. E. Tannenwald, J. Appl. Phys. **30**, S227 (1959).
[7]O. Gaier, J. Hamrle, S. Trudel, B. Hillebrands, H. Schneider, and G. Jakob, J. Phys. D: Appl. Phys. **42**, 232001 (2009).
[8]T. Sebastian, K. Schultheiss, B. Obry, B. Hillebrands, and H. Schultheiss, Front. Phys. **3**, 35 (2015).
[9]S. Demokritov, B. Hillebrands, and A. Slavin, Phys. Rep. **348**, 441 (2001).
[10]N. I. Polushkin, S. A. Michalski, L. Yue, and R. D. Kirby, Phys. Rev. Lett. **97**, 256401 (2006).
[11]H. Ulrichs, B. Lenk, and M. Münzenberg, Appl. Phys. Lett. **97**, 092506 (2010).
[12]H. Yu, G. Duerr, R. Huber, M. Bahr, T. Schwarze, F. Brandl, and D. Grundler, Nat. Commun. **4**, 2702 (2013).
[13]R. Arias and D. L. Mills, Phys. Rev. B **60**, 7395 (1999).
[14]P. Landeros and D. L. Mills, Phys. Rev. B **85**, 054424 (2012).
[15]R. A. Gallardo, A. Banholzer, K. Wagner, M. Körner, K. Lenz, M. Farle, J. Lindner, J. Fassbender, and P. Landeros, New J. Phys. **16**, 023015 (2014).
[16]B. A. Kalinikos and A. N. Slavin, J. Phys. C: Solid State Phys. **19**, 7013 (1986).
[17]See supplementary material at http://dx.doi.org/10.1063/1.4943228 for details regarding film pre-characterization and the numerical calculations.
[18]H. Narisawa, T. Kubota, and K. Takanashi, Appl. Phys. Express **8**, 063008 (2015).
[19]T. Seki, H. Yako, T. Yamamoto, T. Kubota, Y. Sakuraba, M. Ueda, and K. Takanashi, J. Phys. D: Appl. Phys. **48**, 164010 (2015).
[20]T. Sebastian, Y. Ohdaira, T. Kubota, P. Pirro, T. Brächer, K. Vogt, A. A. Serga, H. Naganuma, M. Oogane, Y. Ando, and B. Hillebrands, Appl. Phys. Lett. **100**, 112402 (2012).
[21]J. Sato, M. Oogane, H. Naganuma, and Y. Ando, Appl. Phys. Express **4**, 113005 (2011).
[22]T. Yamamoto, T. Seki, T. Kubota, H. Yako, and K. Takanashi, Appl. Phys. Lett. **106**, 092406 (2015).
[23]A. L. Kwilu, M. Oogane, H. Naganuma, M. Sahashi, and Y. Ando, J. Appl. Phys. **117**, 17D140 (2015).
[24]T. Kubota, S. Tsunegi, M. Oogane, S. Mizukami, T. Miyazaki, H. Naganuma, and Y. Ando, Appl. Phys. Lett. **94**, 122504 (2009).
[25]M. Körner, K. Lenz, R. A. Gallardo, M. Fritzsche, A. Mücklich, S. Facsko, J. Lindner, P. Landeros, and J. Fassbender, Phys. Rev. B **88**, 054405 (2013).
[26]I. Barsukov, F. M. Römer, R. Meckenstock, K. Lenz, J. Lindner, S. Hemken to Krax, A. Banholzer, M. Körner, J. Grebing, J. Fassbender, and M. Farle, Phys. Rev. B **84**, 140410 (2011).
[27]N. Imamura and S. Chikazumi, J. Phys. Soc. Jpn. **24**, 648 (1968).
[28]A. Maksymowicz, J. Whitting, M. Watson, and A. Chambers, Thin Solid Films **197**, 287 (1991).
[29]T. Sebastian, Y. Kawada, B. Obry, T. Brächer, P. Pirro, D. A. Bozhko, A. A. Serga, H. Naganuma, M. Oogane, Y. Ando, and B. Hillebrands, J. Phys. D: Appl. Phys. **48**, 164015 (2015).
[30]W. Y. Choi, H.-J. Kim, J. Chang, S. H. Han, H. C. Koo, and M. Johnson, Nat. Nanotechnol. **10**, 666 (2015).
[31]G.-M. Choi, C.-H. Moon, B.-C. Min, K.-J. Lee, and D. G. T. Cahill, Nat. Phys. **11**, 576 (2015).
[32]S. Urazhdin, V. E. Demidov, H. Ulrichs, T. Kendziorczyk, T. Kuhn, J. Leuthold, G. Wilde, and S. O. Demokritov, Nat. Nanotechnol. **9**, 509 (2014).